2023-01-0792 Published 11 Apr 2023

Impact of Precipitation Drag on a Road Vehicle

Arash Raeesi, Brian McAuliffe, and Joshua Galler National Research Council Canada

Citation: Raeesi, A., McAuliffe, B., and Galler, J., "Impact of Precipitation Drag on a Road Vehicle," SAE Technical Paper 2023-01-0792, 2023, doi:10.4271/2023-01-0792.

Received: 25 Oct 2022 Revised: 11 Jan 2023 Accepted: 25 Jan 2023

Abstract

Road vehicles in the real world experience aerodynamic conditions that might be unappreciated and omitted in wind-tunnel experiments or in numerical simulations. Precipitation can potentially have an impact on the aerodynamics of road vehicles. An experimental study was devised to measure, in a wind tunnel, the impact of rain on the aerodynamic forces of the DrivAer research model.

In this study, a rain system was commissioned to simulate natural rain in a wind-tunnel environment for full-scale rain rates between about 8 and 250 mm/hr. A 30%-scale DrivAer model was tested with and without precipitation for two primary configurations: the notch-back and estate-back variants. In addition, mirror-removal and covered-wheel-well configurations were investigated.

The results demonstrate a distinct relationship between increasing rain intensities and increased drag of the model, providing evidence that road vehicles experience higher drag when travelling in precipitation conditions. At the lowest rain rates examined, representing moderate rain conditions equivalent to about 8 and 29 mm/hr full scale, drag increases on the order of 2% to 4% were measured. Drag increases in excess of 10% were observed for the highest rain rate tested, which represented an unrealistically-high precipitation condition equivalent to about 250 mm/hr full scale. A non-linear increase in drag with rain rate was observed, suggesting that multiple mechanisms of rain-induced drag were present during the experiments. Lift- and side-force variations did not manifest any trends that were beyond the estimated experimental uncertainty. Therefore precipitation is likely not an influence towards aerodynamic stability. Within the experimental uncertainty, the results did not show any evidence of rain affecting the drag changes associated with modifications to the vehicle shape.

Introduction

The aerodynamic drag of a vehicle moving through air is a principal contributor to its road load and subsequently to the power requirement to keep the vehicle in motion. An accurate assessment of absolute drag coefficient resulting from aerodynamic improvements to a vehicle shape is difficult to achieve during wind tunnel experiments due to the complexity of simulating adequately all real-world conditions. A potential aerodynamics-related contributor to the road load of a vehicle is the influence of precipitation, mainly via the interaction of rain with the vehicle body. This influence to road-vehicle road load has yet to be investigated and documented in the public literature. Upon impact, the transfer of momentum from rain droplets to a moving vehicle will add drag to the vehicle, via combined aerodynamic and hydrodynamic phenomena, but it is unknown how to quantify this influence, and whether the influence is sufficient to change the road-load performance of a vehicle.

The impact of precipitation on the aerodynamics of road vehicles is a complex and multi-physics phenomenon, with limited or scarce literature existing on this topic. Nonetheless, aerodynamic influences of heavy rain on aerodynamic performance of aircraft have been studied extensively due to concerns for aviation safety. With respect to road vehicles, studying road-vehicle soiling has become an increasingly important part of the design process within the past decade [1, 2]. That work, although performed for different purposes, involves the same physics and technologies as investigating the impact of precipitation on the aerodynamic performance of road vehicles. It is presumed that the mechanisms impacting aerodynamic performance of aircraft would be essentially similar to those for road vehicles and when combined with the existing knowledge and technologies for road vehicle soiling, it provides a strong basis for a preliminary assessment and approach to the problem of aerodynamic penalties to road vehicle due to precipitation. Raeesi and McAuliffe [3] provide a review of the available literature on the impact of precipitation (rain in particular) on aerodynamic performance of aircraft. Their review is based in large part on studies of aircraft and airfoils under rain conditions [4, 5, 6]. In rain, aircraft wings can

experience loss of lift accompanied with an increase in drag and the possibility for early stall. Three mechanisms were identified in the literature as the main reasons causing aerodynamic performance degradation of aircraft wings:

- As rain droplets impinge on the surface of a moving aircraft wing, a momentum transfer occurs from the droplets to the wing which is opposite to the direction of motion and downward. This momentum transfer decelerates the aircraft or, in order to keep a constant speed, requires more thrust and can be viewed as a source of incremental aerodynamic drag and reduced lift.
- When droplets impinge on the surface of the moving wing, they either stick, rebound, spread, or splash back. This behaviour largely depends on the Weber number regime and it has been shown that at aircraft (and road vehicle) speeds, a significant majority of the droplets either splash back or spread. The splash back produces a cloud of numerous finer particles near the wing surface. These particles accelerate back into the flow and therefore act as a momentum sink for the flow around the wing, especially in the boundary layer causing it to decelerate. This local momentum loss and deceleration can be viewed as another source of aerodynamic drag increase and lift degradation.
- A portion of the droplets spread on the wing surface and form a thin water film. Along the chord of the wing, the water film breaks down into water rivulets which eventually fall off at the trailing edge. The motion and behaviour of the water film is controlled by the balance of surface tension, aerodynamic shear forces, and gravity. This thin water film can acts as local roughness on the wing (especially when it gets wavy) and change the boundary-layer behaviour of the wing causing additional aerodynamic performance degradation.

Of the three mechanisms mentioned above it is conceivable that the first two would be applicable to road vehicles in rain and the third one would be highly dependent on the vehicle shape and may manifest some local or global effects. A preliminary assessment of the momentum-transfer mechanism for road vehicles was provided by Raeesi and McAuliffe [3] by developing an analytical model for momentum transfer. This model provided a preliminary assessment of the magnitude of rain-induced drag for road vehicles. Applying the model for a simplified box-type vehicle demonstrated that the additional drag due to momentum transfer from rain droplets could be significant. For instance, this method predicted a 40% increase in vehicle drag for a heavy rain-fall rate of 100 mm/hr, and 4% drag increase for a moderate rain-fall rate of 10 mm/hr. This preliminary assessment, which only addresses one of the potential precipitation-induced-drag mechanisms, shows the potential importance of further research on this issue in order to reach a more realistic assessment of road-vehicle aerodynamics under precipitation conditions.

Based on the reviewed literature [3], experimental and computational approaches were contrasted. Due to cost, facility limitations, and the necessity to develop new testing capabilities, wind-tunnel testing at subscale was considered as a preferable first step. However, the complex physics of the problem raises important issues that have to be properly considered for subscale testing. A dimensional analysis was performed to examine the non-dimensional groups involved in the scaling of these hydro/aero-dynamic processes of road vehicles under rain conditions. To perform a wind-tunnel test at subscale, rain parameters should also be scaled accordingly but the Reynolds number (flow scaling) and the Weber number (which is the ratio of the inertial forces to the surface tension forces upon the droplet-impact) will not necessarily be preserved and special care should be given to manage the challenges arising from this to preserve the physics of the problem.

In regards to evaluating the magnitude of the potential influence of rain-induced drag on the performance of ground vehicles, Raeesi and McAuliffe [3] considered the following parameters for investigation:

- Vehicle shape/class: Evaluate whether vehicle shape has an influence on the added drag from rain by examining differences in rain-drag effects for a step or slant-back shape such a coupe/sedan configuration, a square-back shape such as an Sports Utility Vehicle (SUV)/ minimvan/hatchback configuration, and a heavy-vehicle shape such as a tractor-trailer combination.
- Precipitation intensity: Evaluate the magnitude of the added rain drag for light, moderate and heavy rain-fall rates.
- Cross winds: Evaluate the precipitation-drag effect under aligned-wind conditions (0°yaw angle) and at least one cross-wind case (in the 5°to 10°yaw-angle range).
- Turbulent winds: Evaluate the precipitation-drag effect under smooth- and turbulent-wind conditions.
- Ground/wind speed. Evaluate how much the precipitation-drag effect changes when the ground speed (oncoming wind speed) is changed, for conditions of moderate to high speeds (between 50 km/hr and 100 km/hr).

Based on these recommendations, a first step towards assessing the magnitude of precipitation-drag impacts on a road vehicle was undertaken using a sub-scale wind-tunnel-testing approach. This preliminary study addresses most of the recommendations listed above, except for light-rain conditions, the use of an HDV model, and the influence of wind-turbulence effects.

Experiments were undertaken in the NRC 3 m × 6 m Propulsion and Icing Wind Tunnel with a 30%-scale road-vehicle model at wind speeds up to 25 m/s (90 km/hr), using a set of water spray nozzles to introduce appropriate water-volume fractions and particle-size distributions into the wind. The model was based on the passenger-car-shaped DrivAer model, with three shape changes examined: 1) changing the back from a notch-back shape to a square-back (estate-back) shape, 2) removing the mirrors, and 3) covering the wheel cavities. With variations in the precipitation rates ranging from light rain to a thunderstorm-level downpour, and variations in the yaw angle up to 15°for some configurations, these model changes were expected to provide some insight about the mechanisms of precipitation drag and the areas of the vehicle most sensitive to its effects (front, back, sides, and extremities).

Experimental Methods

Wind Tunnel

The wind tunnel campaign was carried out in the NRC 3 m × 6 m Wind Tunnel in Ottawa, Canada, shown in Figure 1. This large open circuit wind tunnel has a 7.9 m diameter 16-blade fan that draws outdoor air and pushes it through a large settling chamber followed by a 6:1 contraction ratio. The fan is fitted with a set of anti-swirl stators and the settling chamber has a set of fine-mesh screens to reduce flow turbulence. The wind tunnel has a test section 3.05 m wide, 6.1 m high, and 12.2 m long. A lower insert was installed, that is used to increase the maximum wind speed possible in the test section, and which reduced the test section height to 5.4 m. The test section is followed by a diffuser with a 90° bend and the tunnel exhausts directly outdoors. The fan is powered by a 750 kW DC motor, providing a maximum wind speed on the order of 40 m/s for an empty test section, depending on the insert configuration. The turbulence level of the wind tunnel is less than 1% over the range of wind speeds that were considered.

Test Setup

The experiments were conducted using a surface-vehicle ground-board installation, shown in Figure 2. The ground-board is used for tests of moving surface objects, such as vehicles, because it allows the boundary layer on the wind tunnel floor to be minimized by starting the new boundary layer at the front of the ground-board, that is located 1.57 m upstream of the vehicle centre. The ground-board was installed 0.55 m above the test section floor and spanned the entire width of the test section, mounted to support columns on the floor and rails at the walls. Treatment of the boundary layer in this manner is required to minimize the effects of incorrect relative motions between the wind, vehicle and ground. By minimizing the wind-tunnel boundary layer thickness, adequate simulation of the aerodynamic environment is achieved for all but regions closest to the ground.

A yaw-mechanism was installed in the centre of the ground-board to allow for the vehicle to be rotated along the vertical-axis. A photograph of a model yawed to 10° is shown in Figure 2(b).

FIGURE 1 Aerial view of the the NRC 3 m × 6 m Wind Tunnel.

FIGURE 2 Test-section arrangement.

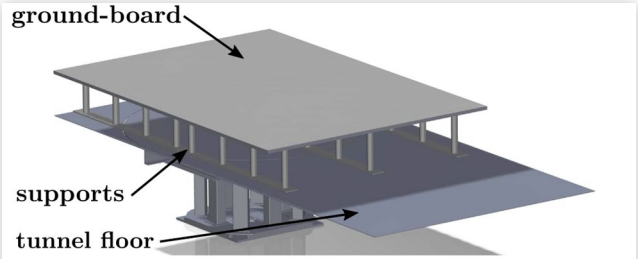

(a) CAD model of the ground-board, showing elevated height off of tunnel floor, and supports used for rigidity.

(b) Wide angle upstream view of test setup

Rain System

Rain conditions were produced using two vertically mounted spray bars separated laterally by 0.76 m, consisting of five nozzles each for a total of ten, shown in Figure 3. A Spraying Systems Co. spray nozzle was selected for rain production (model *SU*4 with fluid cap 60100 and air cap 120). This system uses an air atomizing technique, where a round spray is produced via the external mixing of a jet of air and a jet of water.

In an attempt to achieve a uniform spray at the vehicle longitudinal position and for the wind speeds of interest, the nozzles were arranged vertically 0.152 m apart. The top nozzles

FIGURE 3 Photographs of the rain system and the spray bar setup, displaying the droplets mixing downstream of the nozzles at the maximum flow rate with no background air flow.

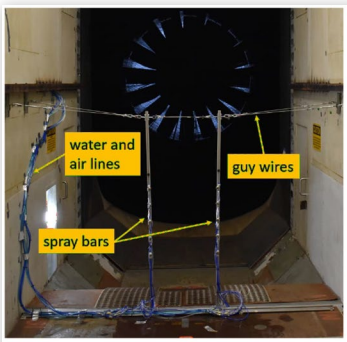

(a) Rain system overall view

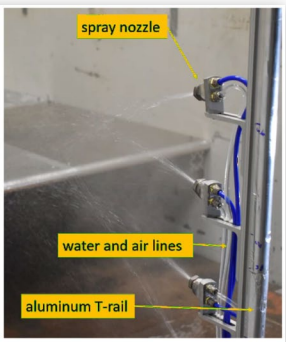

(b) Spray with no wind

were angled 15° downwards while the bottom two nozzles were angled 15° upwards. This would ensure proper mixing of sprays near the model. To wet the desired region surrounding the vehicle model, the lowest nozzle was placed 1.26 m above the tunnel floor and all nozzles were rotated 20° towards the tunnel centre-line, as sketched in Figure 4.

The flow of water and air to the nozzles was controlled using a *rain control panel*. On the water side, the bulk flow was monitored and controlled using two principal flow-meters connected to the main water line and a pressure regulator. For air, a single pressure regulator was used to control the bulk flow. The flow rate through each water and air line was fine-tuned using individual flow-meters (water), pressure gauges (air) and valves, respectively.

Vehicle Models

A 30%-scale model of the DrivAer vehicle shape [7], shown in Figure 5, was used for this investigation. The model built for the current study includes an engine-bay/cooling-flow-path and a detailed underbody, however a closed front grille was used to prevent water penetration into the model. The notch-back (sedan-style) and estateback (station-wagon-style) variants were used for this study.

The model body was manufactured via Selective Laser Sintering (SLS) 3D printing. The modular body pieces, as well as 3D printed wheels were fixed to an aluminum frame that allowed for wheel-height to be adjusted. In addition to an interchangeable back, two additional configurations were tested with the notchback variant: side mirrors removed and wheel wells covered.

Wind loads and moments imparted to the test models were measured with an internal six-component balance. The DrivAer model used an ATI Gamma Series load cell rated for ±130 N in drag and side force, ±400 N in lift, and ±10 Nm for all three moments. This load cell is shown in Figure 6 connected to the streamlined mounting strut along with the positive direction of its three force components F_X, F_Y, F_Z which are along the streamwise, lateral, and vertical directions respectively. The yaw mechanism within the ground-board allowed for measurements to be taken at 4 angles of incidence: 0°, 5°, 10°and 15°.

FIGURE 4 Schematic sketch of the test setup and the rain system. The vehicle model is mounted to the ground-board with the spray bars upstream and angled in order to ensure proper mixing prior to contact with the vehicle.

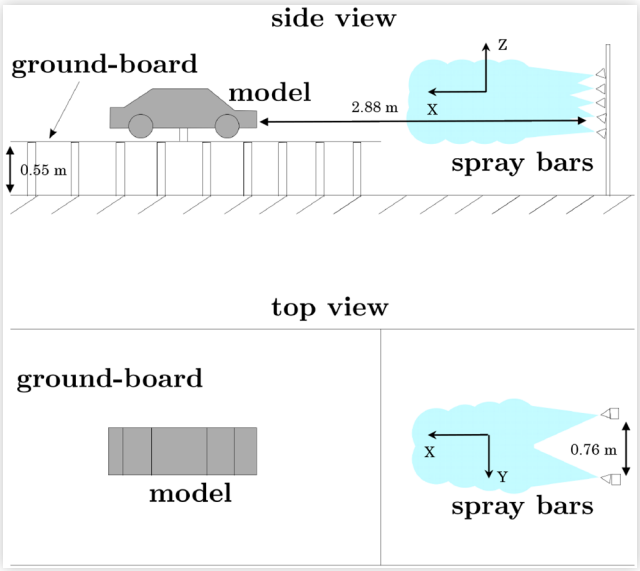

Flow Calibration

A free-stream wind speed of 25 m/s was selected for the majority of test conditions during this campaign. The wind tunnel was calibrated separately for "dry" and "wet" flow conditions using a standard pitot probe and a water-resistant aircraft pitot probe, respectively. The aircraft-probe calibration was unknown, so it was first calibrated against the standard pitot probe in dry conditions, and subsequently used for the wet calibrations. Only a small discrepancy was observed between the dry and wet static-pressure measurements while strong agreement was observed in dynamic pressure which is the variable of interest for calculation of aerodynamic force coefficients. The maximum dynamic pressure discrepancy between the wet and dry calibrations at the test speed of interest was 0.6%. In addition, minimal to no variation was observed on the dynamic pressure between water flow rates, suggesting that any momentum change in the airflow due to the injected spray is negligible. The spray bars and nozzles were mounted in the test section for "dry" and "wet" test conditions, such that any influence from their wakes would be present under all test conditions and act as a common bias error in all measurements.

Rain Characteristics

Droplet Trajectory Modelling

Rain-droplet trajectories were predicted to guide the initial placement of the rain-system spray bars. A free-body diagram for a droplet is shown in Figure 7. A low-order model consisting of force contributions from added-mass and quasi-steady drag was used to predict the resultant drag force [8, 9]. Assuming rigid, spherical rain droplets, Equation 1 was used to determine the droplet drag, $F_D d$, on a single rain droplet:

$$\mathbf{F_D d} = K\rho\frac{4}{3}\pi D^3\mathbf{a_{rel}} + \frac{1}{2}\rho C_{Dd}\mathbf{U_{rel}}^2\pi D^2 \qquad (1)$$

where K is the added mass coefficient, ρ is the density of the air, D is the droplet diameter, $\mathbf{a_{rel}}$ is the relative acceleration between the droplet and the flow, C_{Dd} is the droplet drag coefficient, and $\mathbf{U_{rel}}$ is the relative velocity between the droplet and the flow.

Trajectories along the three coordinate directions shown in Figure 4 were estimated by initializing the droplets at the spray nozzle location and stepping forward in time, updating the droplet kinematics at each time-step. The droplet equation of motion was written as follows:

FIGURE 5 30%-scale DrivAer model configurations.

(a) Notchback configuration

(b) Estateback configuration

(c) Notchback configuration with mirrors removed

(d) Notchback configuration with wheel wells covered

FIGURE 6 Six-component ATI Gamma force balance mounted to the streamlined strut.

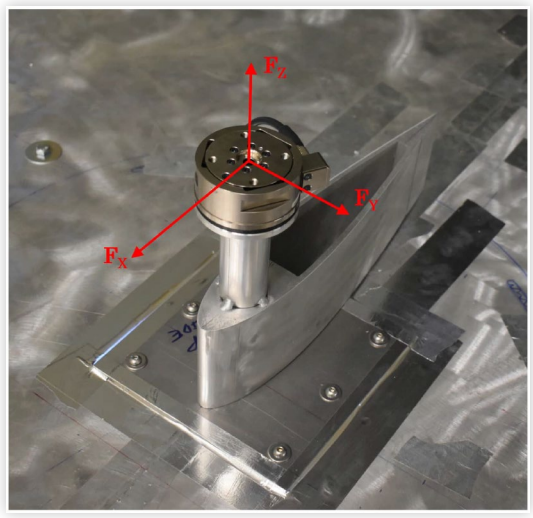

FIGURE 7 Free body diagram for a water droplet released in a background flow.

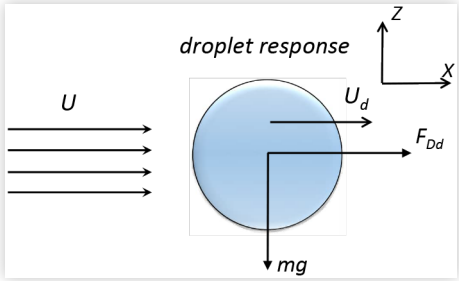

$$ma_x = F_{DdX} \tag{2}$$

$$ma_y = F_{DdY} \tag{3}$$

$$ma_z = F_{DdZ} - mg, \tag{4}$$

where F_{DdX}, F_{DdY}, and F_{DdZ}, are the droplet drag force along the three coordinate directions, m is the mass of a water droplet and g is the acceleration due to gravity. Various nozzle heights were simulated to obtain a predicted distribution of trajectories, based on the range of anticipated droplet sizes. Modelled trajectories for a range of target droplet sizes, as exemplified by Figure 8, were used to guide the placement of the spray bars, optimizing coverage of the vehicle while minimizing droplet spread in the vertical axis. Only minor adjustments to the predicted nozzle placement and orientations were required in the wind tunnel, demonstrating the usefulness of this approach.

Scaling Principles

The parameters affecting the aerodynamic forces of a road-vehicle under rain precipitation were described in detail by Raeesi and McAuliffe [3] based in large part on the work of

FIGURE 8 Modelled trajectories for water droplets of diameters from 0.5 mm to 5 mm. The black box indicates the vehicle position upstream.

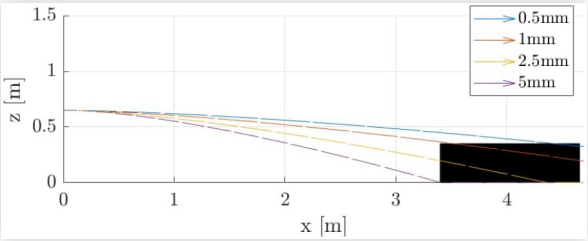

Belanin et al. [10]. The scaling laws were employed in the study and the non-dimensional groups controlling the physics of the rain-induced drag of a scaled vehicle model were derived. Those non-dimensional groups pertaining to rain generation systems are:

$$\frac{l}{L} \tag{5}$$

$$\frac{D}{L} \tag{6}$$

$$\frac{\rho U^2 D}{\sigma} = We \tag{7}$$

where l is the average spacing between the rain particles, L is the characteristic length of the vehicle, D is a representative droplet diameter, ρ is the air density, U is the resultant wind speed that the vehicle experiences (i.e. the wind tunnel speed for this study), and σ is the surface tension between the air and water. Equation 7 represents the Weber number, We, which is the ratio of inertial forces to the surface tension. Therefore, in order to perform high fidelity and representative experiments to simulate the impact of rain on a scaled vehicle model, these three groups are to be preserved. The average distancing between the rain droplets is directly proportional to the Liquid Water Content (LWC) of the rain which is also directly proportional to the rain rate. Therefore, the objective of generating a representative rain in the wind tunnel was to scale down the rain rate and the droplet sizes to the same ratio of 30%. It is apparent from the Weber number equation that when scaling the droplet sizes to 30% for this experimental setup without increasing the wind tunnel speed (which was not possible due to limits on wind speed associated with the experimental setup), the Weber number would not be preserved. This was shown to be the case in the preliminary study [3]. The range of Weber numbers for both scaled and full-scale cases are within the range 1.8×10^3 to 4×10^4. At this We range, the predominant behaviour of droplets upon impacting a solid surface is to splash [3]. This suggests in both scaled and full-scale cases the droplets show predominantly similar behaviour upon impingement on the solid surface, and therefore the scaled tests would be physically representative of the full-scale phenomenon.

Rain Rate Measurements

The rain rate was measured and calibrated using a collection-based method. The method is based on an assumption that the vertical motion of the droplets is that which relates to the precipitation-rate condition in the ground-referenced coordinate system through which the vehicle moves, which is equivalent to a moving wind-referenced coordinate system in the wind tunnel. With only horizontal motion differentiating these two coordinate systems, the vertical accumulation of water in the stationary-ground environment should be the same as that in the wind-tunnel environment. The overall wetted area of the ground-board was affected by wind speed, becoming larger with increasing rain rate, and with droplets remaining entrained in the air flow past the ground-board at higher flow rates. Therefore, the water flow rate is not necessarily proportional to the effective stationary-ground rain rate. The water spray was collected by trays installed over the wetted area of the ground-board for different spray-system flow rates to measure the vertical accumulation over a period of time. The trays were placed at various locations near the vehicle-model location to provide a reasonable measure of the rain rate experienced by the vehicle model once installed at a later time. An average of the accumulated rain in each tray was used to define the rain rate.

Table 1 outlines the rain-rate magnitudes used for this investigation. The terms "low", "medium", "high", and "highest" refer to these rain conditions used during the test campaign. The "highest" rain rate is an extremely violent rain rate that is not sustainable in nature for longer periods of time. Uncertainty associated with the rain-rate magnitude is estimated to be ±15% of the stated values, based on the tray-collection-based calibration method, and the possible day-to-day variability due to evaporation within the test section. Repeatability of the rain-rate conditions using the rain-control panel was anticipated to be better than this ±15% magnitude error, however a quantification of the random error was not possible based on the limited data acquired. The vehicle-model test data presented in this paper were acquired on a single day for which the relative humidity varied between 85% and 95% through out the day, a level for which evaporation was not anticipated to affect the rain rates between test runs.

Rain Droplet Size Distribution

The rainfall droplet-size-distribution model of Marshall and Palmer [11] was used to define the droplet-size distribution corresponding to the rainfall rates of Table 1. The full-scale distributions associated with the three realistic rain rates are

TABLE 1 Rain rates measured in the wind tunnel, their respective water flow rates, and equivalent full scale rain rates.

Rainfall Type	Water flow rate [liter/min]	Rain rate [mm/hr]	Full scale rain rate [mm/hr]
Low	0.2	2.4 ± 0.4	8 ± 1.2
Medium	0.6	8.7 ± 1.3	29 ± 4.4
High	2	23 ± 3.4	75 ± 11
Highest	6.6	75 ± 11	250 ± 38

shown in Figure 9. The droplet-size distribution is presented by means of the volume frequency (%) for the range of droplet sizes. The volume frequency for a droplet size, D, represents the ratio of the volume of water comprised of total number of droplets with diameter D to the total volume of water. In Figure 9, the Volume Frequency is shown against the range of droplet sizes in microns (μm). It is shown that, with increasing rain rate, the distribution curve is widened and skewed toward the larger particles which is the expected behaviour during heavier rainfalls. For each droplet-size distribution, a few important representative values can be extracted from the distribution. The average volumetric droplet size, D_{va}, is the diameter corresponding to the average volume of water obtained from dividing the total volume of water by the total number of particles. The median droplet diameter of the distribution is represented by $D_v(50)$ whereas $D_v(10)$, and $D_v(90)$ are the 10*th* and 90*th* percentiles i.e. droplet diameters that are larger than 10% and 90% of the total number of droplets respectively.

A Malvern Panalytical Spraytec laser diffraction system was used to measure the droplet size distribution of the flow [12]. This measurement device works based on the principle of laser diffraction. A laser beam transmitted by the emitter side is passed through a spray cloud and laser beam is diffracted due to the presence of liquid droplets. The receiver has a lens that focuses the diffracted laser beam on a series of detectors where the intensities of light are measured. Droplet-size distribution is related to the recorded light intensities and is obtained using the pre-calibrated system. The measurement devices were mounted on an optical rail and fixed to the ground-board at a location coincident with the vehicle model that would later be installed. The setup is shown in Figure 10. Two steel canisters were used to shield the emitter and receiver modules and as waterproofing to protect against water intrusion during the tests. Two small cut-outs on the side walls of the canisters allowed the laser beam to be transmitted through the spray cloud and received on the other end.

FIGURE 10 Malvern system inside of steel waterproofing canisters. Cut-outs in the canister walls allowed for the laser emitter to reach the receiver while protecting the rest of the equipment from the water spray.

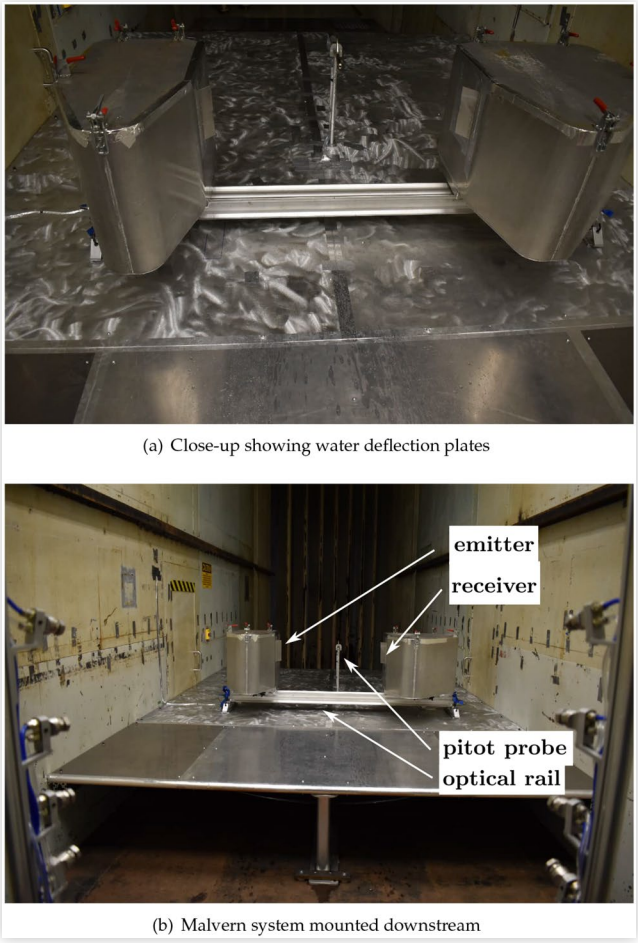

(a) Close-up showing water deflection plates

(b) Malvern system mounted downstream

FIGURE 9 Droplet size distribution for flow rates representative for equivalent low, medium, and high rain test conditions.

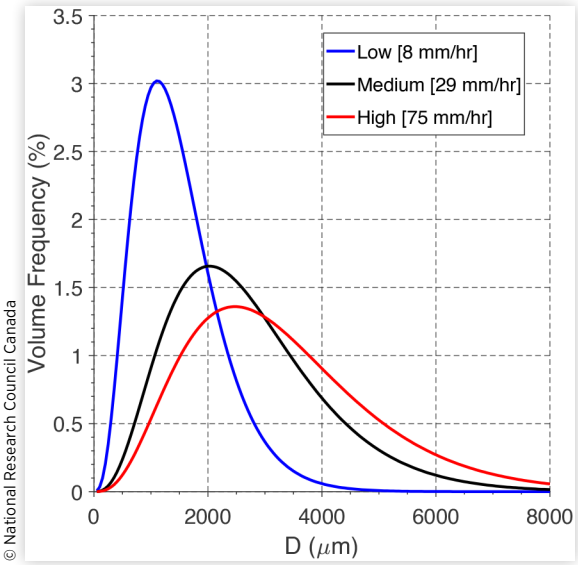

Several adjustments and tuning to the location of spray nozzles were made using real-time Malvern measurements to maximize the spray cloud passage across the laser beam. Measurements were conducted for the calibrated rain rates and the droplet size distributions were analyzed. The results are presented in Figure 11 for the four calibrated rain rates. The general trend of widening of the probability distribution curves can be seen when increasing the rain rate from low to high. The measurement limitations of the Malvern system, which can measure droplet sizes between 2 and 2000 microns for the 75 mm focal-length lenses used, results in a non-smooth distribution profile above 2000 microns for the Medium, High, and Highest rates. The target distributions, based on the Marshall and Palmer model [11] scaled by 30%, are also presented in Figure 11. For each rain rate, the measured distributions are shifted to larger particle sizes than the target distribution. Based on these results, the average volumetric droplet sizes and the percentile values were calculated and are presented in Table 2, with the target values calculated from the Marshall and Palmer model.

FIGURE 11 Droplet size distribution measurements for the calibrated rain rates using the Malvern system

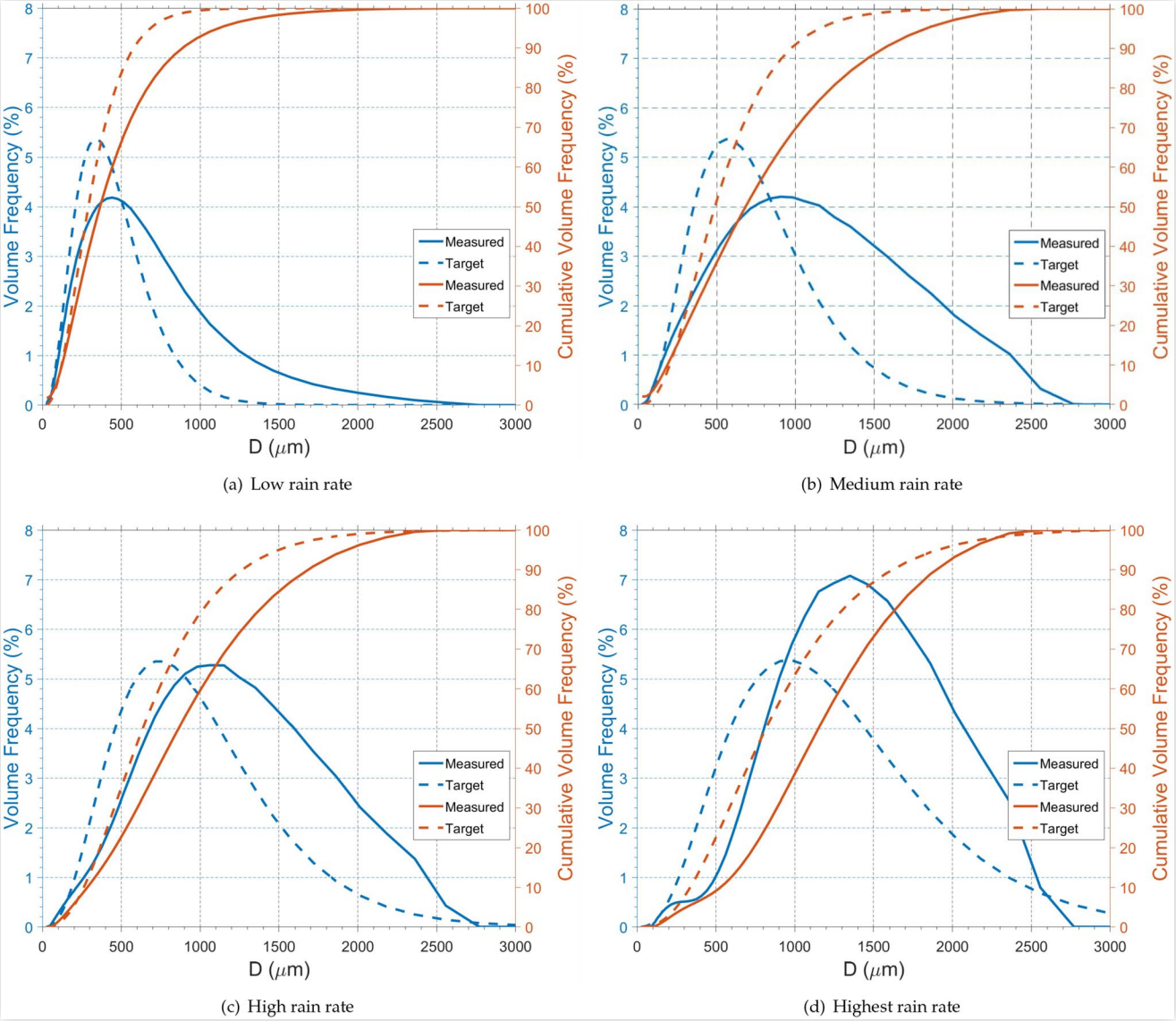

TABLE 2 Measured and target values for the representative droplet diameters

Rain rate	D_{va}	$D_v(10)$	$D_v(50)$	$D_v(90)$
Measured Values [μm]				
Low	272	134	377	906
Medium	433	199	714	1585
High	1232	297	906	1716
Highest	1434	562	1152	2013
Target Values [μm]				
Low	226	135	293	534
Medium	392	252	534	984
High	473	411	864	1455
Highest	1540	555	1155	2055

There is reasonably good agreement between the target values obtained from the model and the measured values, especially for the higher rain rates. However, it may be expected the actual distribution of droplet sizes in the wind tunnel would have been slightly shifted toward the larger sizes, had the measurement system been capable of measuring larger droplet sizes. For low and medium rain rates the deviation between measured and target $D_v(90)$ values is large, as is evident from the distributions of Figure 11. This is likely related to the larger spray nozzle openings and the fact that, even at lower flow rates and higher atomizing air pressures, large particles are still generated. For future testing, by choosing smaller spray fluid nozzles for lower rain rates, this issue could be rectified.

Results

Wind tunnel tests were conducted for the DrivAer model in both Notchback and Estateback configurations over a range of wind speeds, yaw angles, and rain intensities. The effect of

removing side mirrors and covering the wheel wells were also investigated for the Notchback model. The complete test matrix is presented in Table 3.

The aerodynamic force coefficients were calculated from the ATI load cell's X, Y, and Z force components measured during the tests. The X component is along the model longitudinal direction, Y component is along the model lateral direction, and Z component is along the vertical direction (see Figure 4). Aerodynamic force coefficients are defined in Equations 8 to 10 where the drag force, side force, and the lift force are represented by C_D, C_S, and C_L respectively. In these equations, A is the frontal area of the model, U is the wind tunnel speed, ρ is the air density in the wind tunnel test section and F_X, F_Y, and F_Z are the three body-aligned force components acquired from the load-cell measurements as they were shown in Figure 6.

$$C_D = -\frac{2F_X}{\rho U^2 A} \tag{8}$$

$$C_S = -\frac{2F_Y}{\rho U^2 A} \tag{9}$$

$$C_L = -\frac{2F_Z}{\rho U^2 A} \tag{10}$$

The tests were carried out at a wind tunnel speed of 25 m/s to match the Reynolds number (Re) of tests previously conducted for the same model at 15%-scale in NRC 2 m × 3 m Wind Tunnel Wind Tunnel [13]. To ensure the aerodynamic behaviour of the model is independent of Re effects at this speed, speed sweep tests in dry conditions were performed to validate the independence of drag force coefficient with the wind speed. The variation of drag force coefficient with the wind-tunnel speed is shown in Figure 12. In the range 20 m/s to 30 m/s, the uncertainty of C_D is about ±0.003 (confidence interval is about 1.5 × the symbol diameter) and therefore the results reveal that the drag force under dry conditions is essentially independent from the wind speed in this range.

TABLE 3 Test Matrix

Model	Configuration	Test Type	Wind Speed [m/s]	Yaw Angles [°]	Rain rates [mm/hr]
Notchback	Baseline	Dry Reynolds sweep	10, 15, 20, 25, 30	0	0
		Rain rate variation	25	0, 10, 15	0, 8, 29, 75, 250
	Wheel wells covered	Rain rate variation	25	0, 10, 15	0, 29, 75, 250
	Side Mirrors off	Rain rate variation	25	0, 10, 15	0, 29, 75, 250
Estateback	Baseline	Rain rate variation	25	0, 5, 10, 15	0, 29, 75, 250
		Reynolds number sweep	15, 20, 25	0	0, 29, 75, 250

FIGURE 12 Drag force coefficient versus wind speed for DrivAer Notchback model

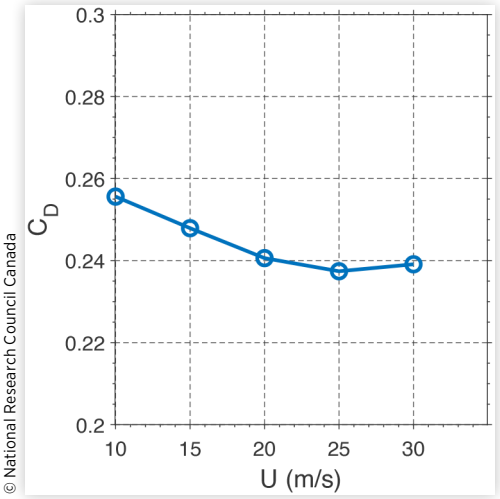

The obtained results in dry conditions were validated against previous results conducted in the NRC 2 m × 3 m Wind Tunnel Wind Tunnel using a 15%-scale DrivAer model with both Notchback and Estateback configurations [13], the results of which are compared in Figure 13. There is a good agreement for the drag force and side force coefficients between the current study and the 15%-scale model results with the closed-cooling configuration, suggesting that the experimental setup, including the presence of the spray bars, provides an appropriate set of baseline dry-condition results. In the current study, a closed front grill (closed cooling) configuration was used to prevent water permeation into the insides of the model and to protect the load cell instrument. The 15%-scale tests were performed for both closed and open cooling and the significant impact of the cooling airflow in the engine cavity on the aerodynamic drag can be realized from the data presented. The agreement between the lift force coefficient behaviour was worse than the drag and side force coefficients. In the current study the lift force was consistently higher than that of 15%-scale model tests. The reason behind this observation is not clear; however, one possible reason may be related to differences in ground board installation mechanism and the lack of boundary-layer suction for the 30%-scale tests.

The impact of rain intensity on the Notchback and Estateback variants of the model are shown in Figure 14. The results are presented for three yaw angles of 0°, 5°, 10°, for the Notchback model and an additional 15° for the Estateback model. The rain rates shown in the figure are the full scale equivalent rain rates varying from 8 mm/hr (low) to 250 mm/hr (highest) for both models. The error bars shown are based on the uncertainties in both force-coefficient measurement (vertical error bars) and the rain rate measurements (the horizontal error bars). The uncertainty in the force coefficient measurements is estimated from the uncertainties associated with the load cell instrument, its repeatability, and the uncertainties in the wind tunnel dynamic pressure calculations

FIGURE 13 Validation of results with a previous study for DrivAer 15% scale model [14]. Current study results have the "30% closed cooling legend".

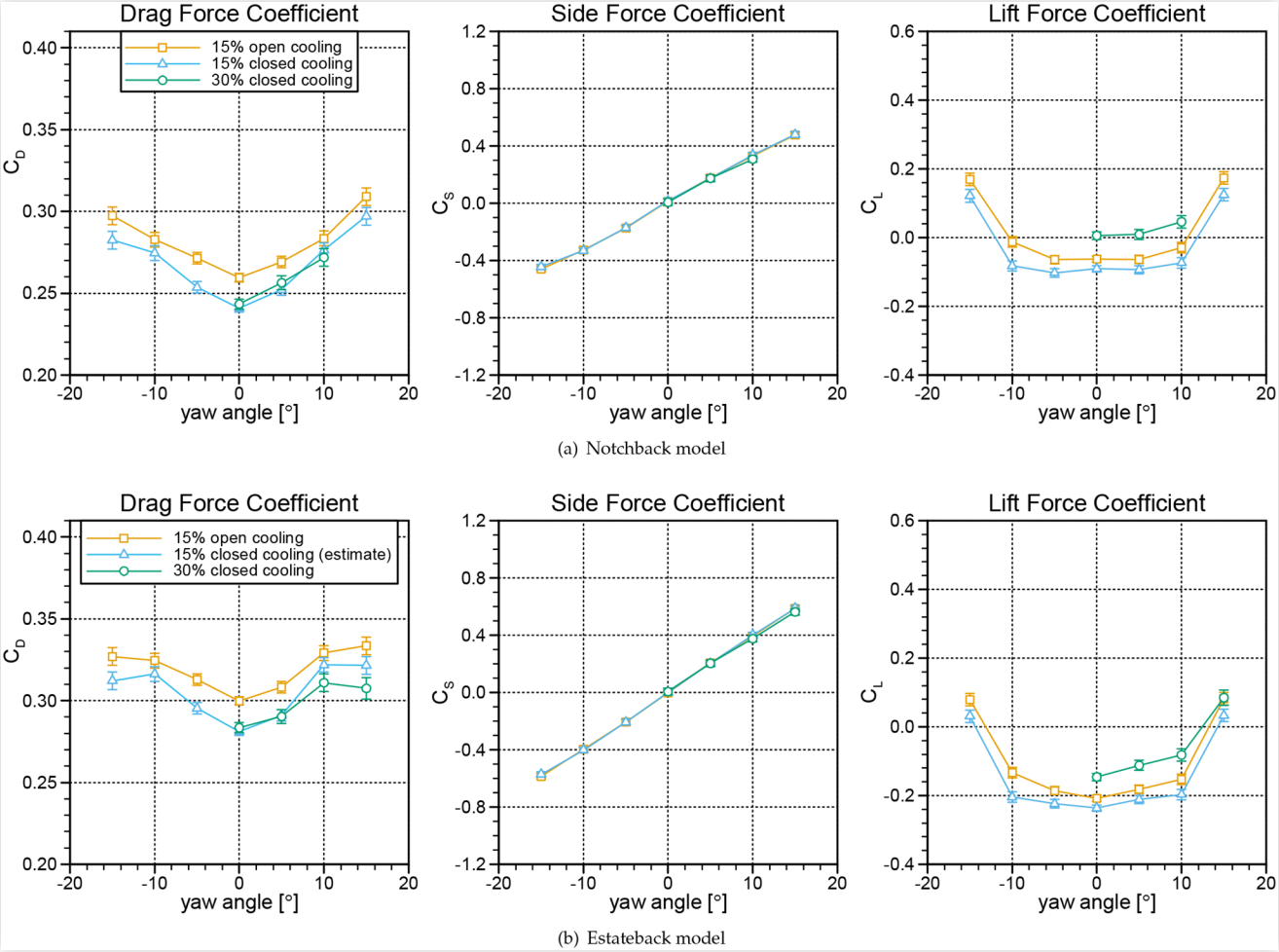

(between ±0.003 and ±0.013 depending on the yaw angle and precipitation condition). The uncertainties in rain-intensity measurements consider the rain-panel flow-meter resolution, an estimated uncertainty in the measurement of the wetted area when the rain rates were calibrated, and possible evaporation within the test section (±15% estimated total uncertainty). The results indicate that there is a clear increasing trend in the drag force with increasing rain intensity for all yaw angles. From dry conditions to the highest rain rate, the increased level in the drag-force coefficient is beyond the magnitude of the error bars, indicating that rain increases the drag force coefficients of the tested models. For side force, a trend appears at higher yaw angles of 10° and 15° where the side force increases with increasing rain intensity. This trend is more apparent for the Estateback model since, due to its larger side area, more vehicle surface area is directly exposed to the rain droplets impingement. These increased levels are, however, within the range of experimental uncertainties shown, so despite the observed trend it cannot be concluded that the side-force coefficient definitively increases with rain rate. No clear trends of lift force varying with rain intensities can be seen from the data presented.

Figure 15 presents the same data as Figure 14 but plotted with respect to yaw angle for different rain rates. From the graphs in Figure 15 it is evident that the increases in drag force coefficients are larger than experimental uncertainties but those for side force and lift force are within the experimental uncertainties.

With the development of new technologies to replace the side mirrors, it is worthwhile to investigate the drag reduction benefits of such technologies under precipitation conditions to examine whether there is any additional or compound effects on the aerodynamic forces in the presence of rain. Previous studies have shown that removing side mirrors can lead to a 2% to 4% reduction in the drag area of road vehicles [15]. This test was only performed for the Notchback DrivAer model, shown in Figure 5c. The results of this test are presented in Figure 16. The absolute C_D, C_S, and C_L values without the side mirrors are presented in Figure 16a whereas the delta values, which are the difference between the tests with and without side mirrors, are shown in Figure 16b. The negative delta values indicate a reduction in aerodynamic forces happened due to removing the side mirrors. Within the experimental uncertainty, the lift and side force coefficient did not

FIGURE 14 Impact of rain intensity at the aerodynamic forces of the 30% scale DrivAer model at different wind yaw angles

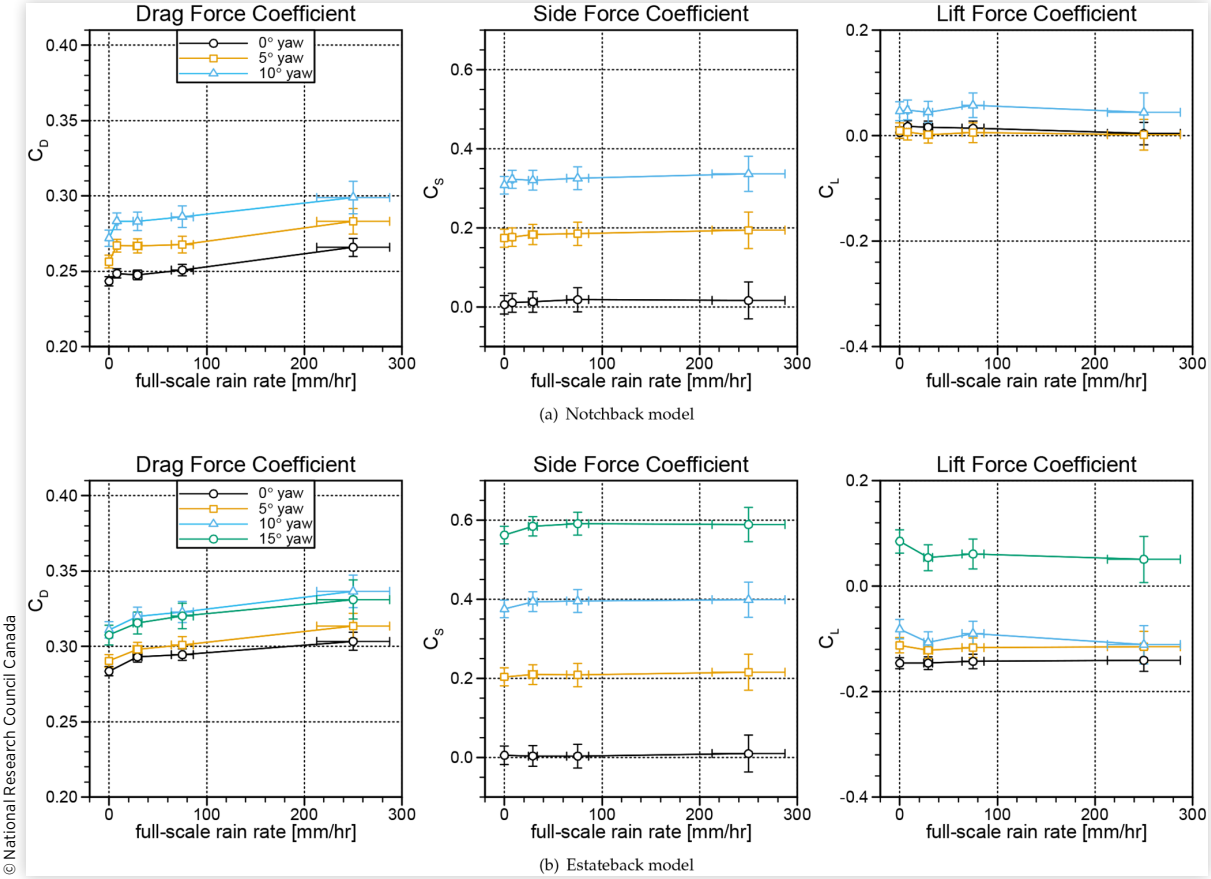

FIGURE 15 Impact of wind yaw angle on the aerodynamic forces of the 30% scale DrivAer model at different rain intensities

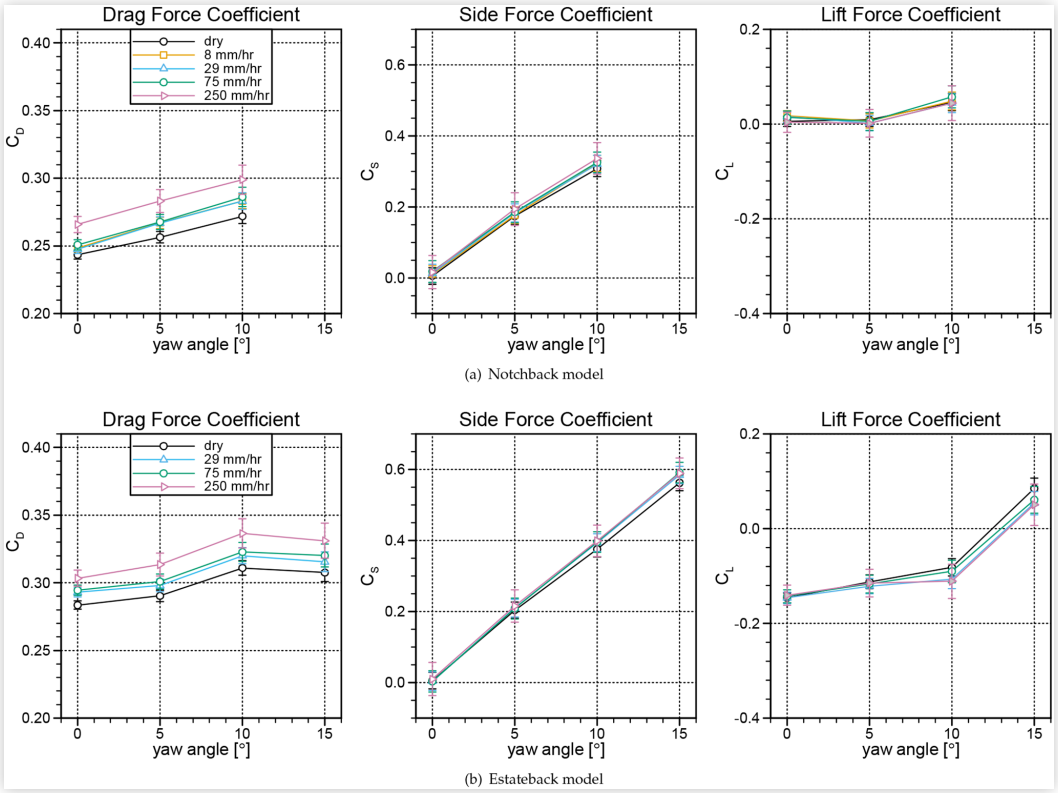

FIGURE 16 Impact of removing side mirrors on the aerodynamic force of the 30% scale DrivAer notchback model

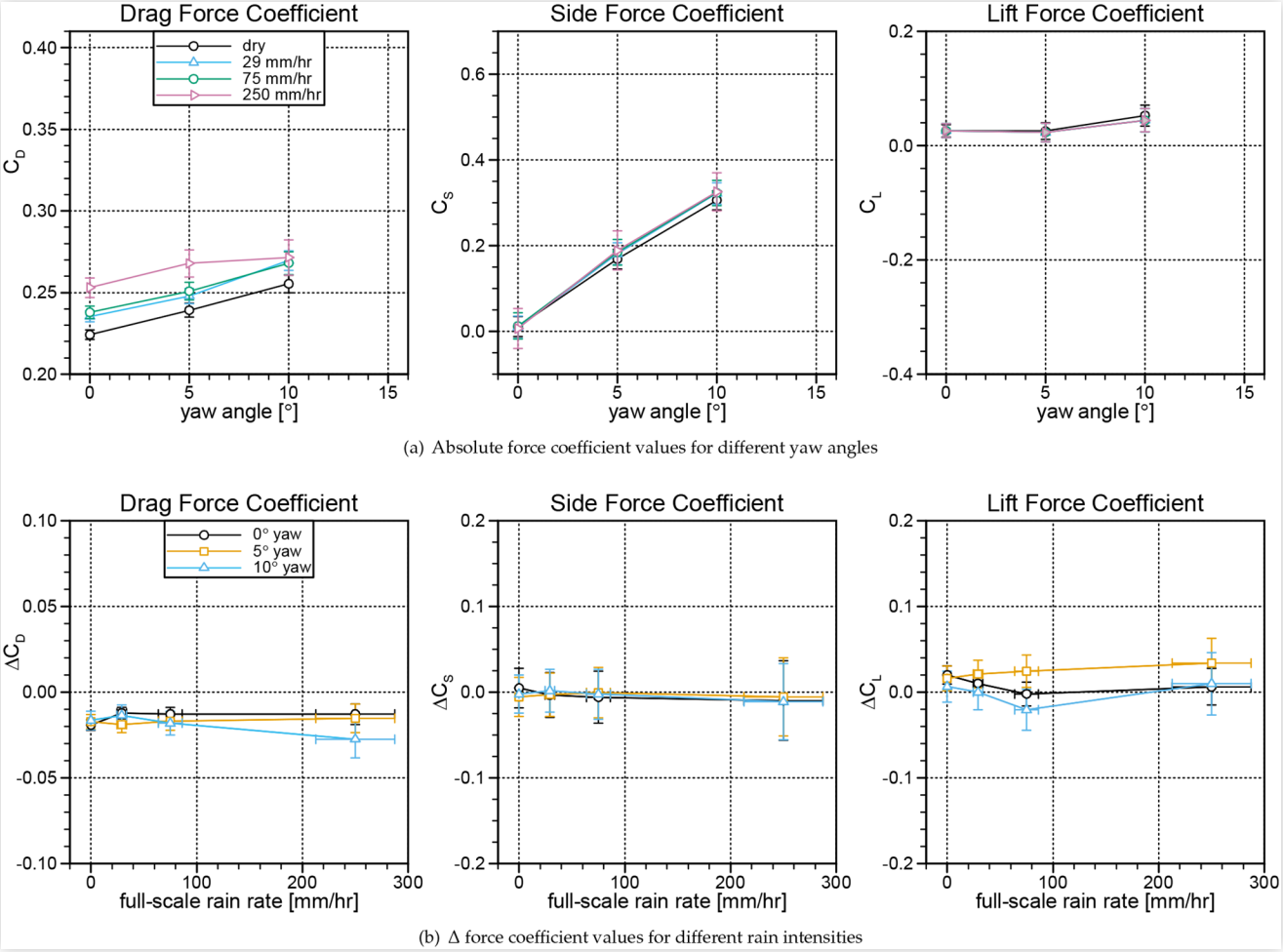

show any additional effect due to the variation of rain intensity whereas the drag force seemed to experience an additional reduction at the highest rain rate when at 10° yaw angle, however the difference is within the uncertainty bounds.

The wheel wells and tires of road vehicles contribute to the total aerodynamic drag. Technologies that reduce aerodynamic-drag contribution of the wheel wells are receiving attention in the automotive industry [16]. In this study, as an ideal case, the wheel wells of the Notchback DrivAer model were completely covered with aluminum tape above the vehicle-underbody height, as shown in Figure 5d. The objective of this test was to investigate whether the covered wheel wells can cause any additional or compound impacts on the aerodynamic forces in the presence of rain. In a real on-road condition, the wheels would be spinning, introducing complex water-spray interactions with the oncoming wind and rain, which is not simulated here. The intent of the wheel-well covers was primarily to examine an aerodynamic body change that would have an influence on vehicle drag and side force in cross-wind/yawed conditions, not necessarily to examine a technology that would influence realistic rain and spray patterns surrounding a vehicle. These tests were conducted for 0°, 5°, and 10° yaw angles and for the medium, high, and the highest rain rates. The results are show in Figure 17. While the ΔC_D results of Figure 17b show that side force increases at the highest yaw-angle of 10° as a result of covering the wheel wells, no quantifiable change in C_D, C_S, or C_L with rain rate is observed, based on the experimental uncertainty.

The results presented in this section show a clear correlation between the aerodynamic drag of the models tested and the presence of rain. This was the case even for the lowest full-scale rain rate of 8 mm/hr, which can be considered a light to medium rain intensity, for which the drag of the vehicle model increased by 2% to 4% depending on the configuration and yaw angle. The overall trend of increasing model drag with increasing rain rate was presented in Figure 14 and shows increases in drag at the highest rain rate (250 mm/hr) in excess of 10%. This dependency between the rain rate and the drag may be affected by other factors. For instance, increasing the rain rates was achieved by turning on more spray nozzles and thus increasing the flow rate. At different rain rates the distribution of droplet sizes varied as shown in Figure 11 and this could change the entrainment of the rain particles by the airflow and thus the proportion of droplets that impinge on the vehicle. Despite this potential uncertainty, the distinct and repeatable trends at each yaw-angle condition and the care taken to generate representative rain-droplet

FIGURE 17 Impact of covering wheel wells on the aerodynamic force of the 30% scale DrivAer notchback model

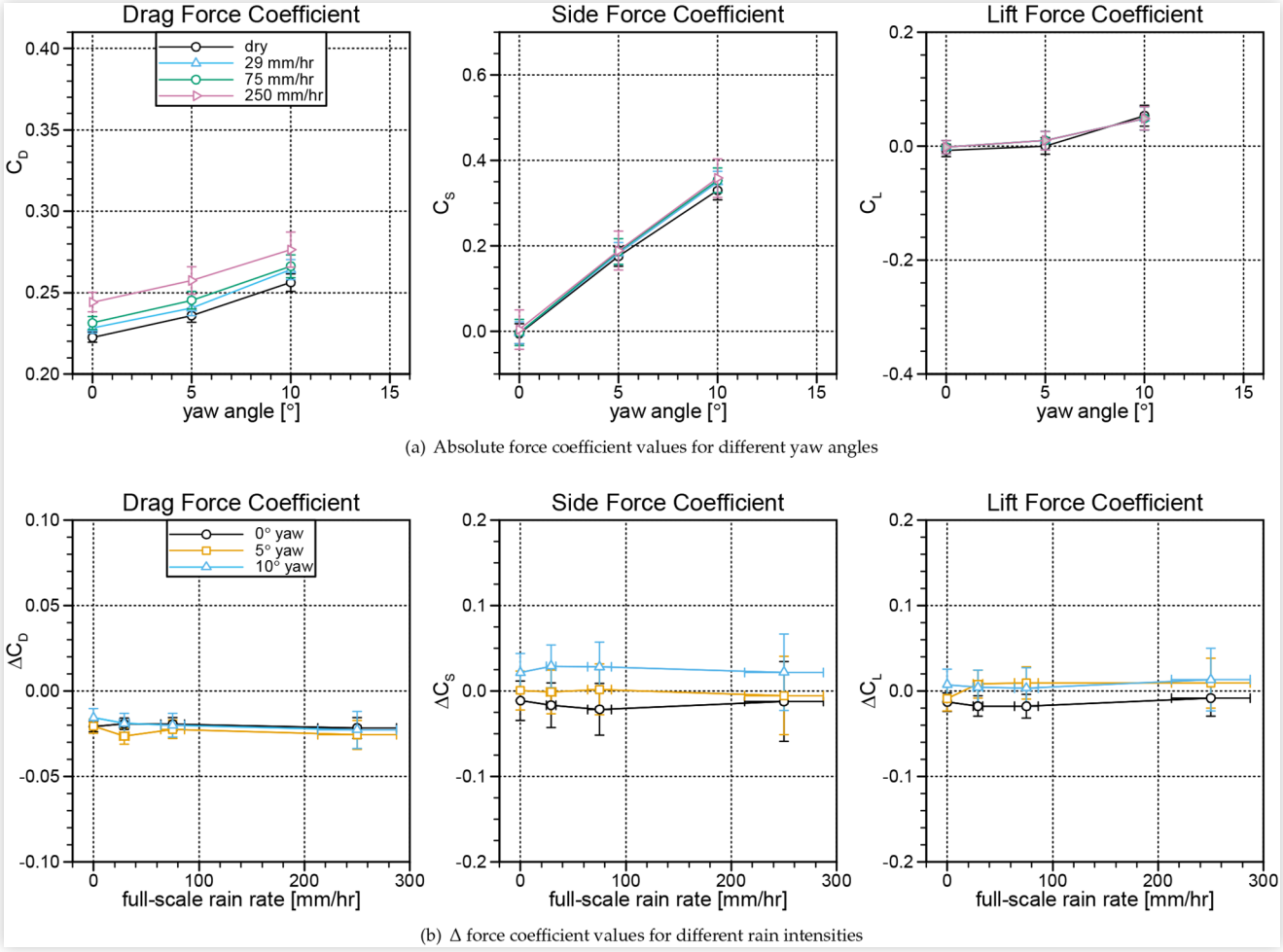

distributions suggest the trends are representative of real-world conditions.

The possible mechanisms of rain impacting the aerodynamics of road vehicles were previously discussed in the introduction. The contribution of each of the three mechanisms (droplet momentum transfer, droplet/boundary-layer interaction, and surface droplet/water-film behaviour) to the total added "rain drag" is unclear. However, some insight may be gleaned from the results based on basic physical principles. At lower rain rates the amount of impinging and splashing droplets are comparatively less and it may be deduced that the momentum transfer and boundary layer momentum loss would have less contribution to the total added drag, while the added surface roughness from the water film might be the primary factor. This may be the reason behind the apparent step increase of the drag from dry to low-rain-rate conditions. As soon as some rain is present there would be small water droplets and rivulets attached to and moving on the vehicle surface that could result in increased friction drag and/or premature flow separation resulting in increased pressure drag. With increasing rain rates, the relative contribution of momentum transfer and momentum loss of the boundary layer should increase. Further research is required to understand the relative strength of each of these mechanisms, and the influence of rain on the aerodynamic behaviour of other vehicle shapes such as pickup trucks and larger medium-duty and heavy-duty vehicles.

Conclusions

The impact of rain precipitation on the aerodynamic behaviour of a 30%-scale DrivAer model with Notchback and Estateback configurations was investigated in the NRC 3 m × 6 m Wind Tunnel. The model was installed on a ground board to reduce the wind-tunnel-floor boundary-layer effects, and precipitation was generated by a rain system located inside the tunnel upstream of the ground board. The test results under dry conditions were validated against previous studies of the same models at 15% scale in a different NRC facility and showed good agreement. In the presence of rain, the results showed that there is a clear relation between increasing rain intensity and the aerodynamic drag of the vehicle, with increases in drag up to 4% at the lowest rain rate tested, and increases in excess of 10% at the highest rain rate tested, suggesting that rain-induced drag has an influence on the energy use and greenhouse-gas emissions of road

transportation systems. Lift and side force variations did not manifest any trends that were beyond the estimated experimental uncertainty, and therefore precipitation is likely not an important influence towards aerodynamic stability. The test results did not show any conclusive evidence of rain affecting the drag changes associated with modifications to the vehicle shape (Notchback to Estateback), removing the side mirrors, or covering the wheel wells, likely because any such changes were within the experimental uncertainty. These results suggest that the influence of rain-induced drag is sufficiently small for component changes such that its influence is not important to consider for aerodynamic optimization.

This study identified a measurable impact of precipitation on the drag of road vehicles, but was limited in scope. In order to understand the influence of rain-induced drag for any road-vehicle shape, further research is required to understand the magnitudes of the different physical mechanisms responsible for the observed behaviour, and to understand the influence on other vehicle shapes such as HDVs. In addition, a focus should be placed on providing predictions of the added fuel/energy consumption and increased greenhouse-gas emissions of road vehicles in the presence of rain.

Acknowledgements

This work was co-funded by Transport Canada's ecoTECHNOLOGY for Vehicles program and the National Research Council Canada's Clean and Energy Efficient Transportation program. The views and opinions of the authors expressed herein do not necessarily state or reflect those of Transport Canada.

References

1. Hagemeier, T., Hartmann, M., and Thévenin, D., "Practice of Vehicle Soiling Investigations: A Review," *International Journal of Multiphase Flow* 37, no. 8 (2011): 860-875.
2. Kabanovs, A., Varney, M., Garmory, A., Passmore, M. et al., "Experimental and Computational Study of Vehicle Surface Contamination on a Generic Bluff Body," SAE Technical Paper 2016-01-1604, 2016, 10.4271/2016-01-1604.
3. Raeesi, A. and McAuliffe, B., "Preliminary Investigation of the Impact of Precipitation on the Aerodynamics of Road Vehicles," NRC Technical Report LTR-AL-2020-0045, National Research Council Canada, 2020.
4. Bilanin, A.J., "Scaling laws for testing airfoils under heavy rainfall," *Journal of Aircraft* 24, no. 1 (1987): 31-37.
5. Hansman, R.J. Jr. and Craig, A.P., "Low Reynolds Number Tests of NACA 64-210, NACA 0012, and Wortmann FX67-K170 Airfoils in Rain," *Journal of Aircraft* 24, no. 8 (1987): 559-566.
6. Bezos, G.M., Dunham, R.E. Jr, Gentry, G.L. Jr, and Melson, W.E. Jr "Wind Tunnel Aerodynamic Characteristics of a Transport-Type Airfoil in a Simulated Heavy Rain Environment." NASA Technical Paper NASATP-3184, NASA, 1992.
7. Heft, A.I., Indinger, T., and Adams, N.A., "Introduction of a New Realistic Generic Car Model for Aerodynamic Investigations," SAE Paper 2012-01-0168, 2012, https://doi.org/10.4271/2012-01-0168.
8. Schiller, L., "A Drag Coefficient Correlation," *Zeit. Ver. Deutsch. Ing.* 77 (1933): 318-320.
9. Reehorst, A.L., "Study of Water Droplet Trajectories in the NASA Lewis Research Center Icing Research Tunnel (IRT)," Nasa Technical Report, 1996.
10. Bilanin, A.J., Quackenbush, T.R. and Feo, A. "Feasibility of Predicting Performance Degradation of Airfoils in Heavy Rain," 1989.
11. Marshall, J.S. and Palmer, W.M.K., "The Distribution of Raindrops with Size," *Journal of Meteorology* 5, no. 4 (1948): 165-166, doi:10.1175/1520-0469(1948)005<0165:TDORWS>2.0.CO;2.
12. Triballier, K., Dumouchel, C., and Cousin, J., "A Technical Study on the Spraytec Performances: Influence of Multiple Light Scattering and Multi-Modal Drop-Size Distribution Measurements," *Experiments in Fluids* 35, no. 4 (2003): 347-356.
13. McAuliffe, B.R. and Barber, H., "Aerodynamic Drag of Road Vehicles in Close Lateral Proximity," Submitted to SAE WCX 23 23SS-0194, 2023.
14. McAuliffe, B.R. and Barber, H., "Aerodynamics of Road Vehicles in Real-world Conditions - Progress Report - Traffic Aerodynamics Phases 2 and 3," NRC Report LTR-AL-2020-0007, National Research Council Canada, 2021.
15. De Souza, F., Raeesi, A., Belzile, M., Caffrey, C. et al., "Investigation of Drag Reduction Technologies for Light-Duty Vehicles Using Surface, Wake and Underbody Pressure Measurements to Complement Aerodynamic Drag Measurements," *SAE Int. J. Adv. & Curr. Prac. in Mobility* 1, no. 3 (2019): 1233, doi:https://doi.org/10.4271/2019-01-0644.
16. Cavusoglu, O.M., "Aerodynamics around Wheels and Wheelhouses," Master's thesis, Chalmers University, 2017.

ISSN 0148-7191